Sensors and Actuators B 208 (2015) 339–345

Contents lists available at ScienceDirect

Sensors and Actuators B: Chemical

journal homepage: www.elsevier.com/locate/snb

Approach for quantification of metal oxide type semiconductor gas sensors used for ambient air quality monitoring

N. Masson*, R. Piedrahita, M. Hannigan

University of Colorado Boulder, Department of Mechanical Engineering, 427 UCB, 1111 Engineering Drive, Boulder, CO 80309, United States

ARTICLE INFO

Article history:
Received 29 June 2014
Received in revised form 4 November 2014
Accepted 7 November 2014
Available online 15 November 2014

Keywords:
Gas sensor
Metal oxide
Metal-oxide quantification
MOx model
Collocation

ABSTRACT

Metal oxide type (MOx) sensors are one of several technologies being employed in low-cost air quality monitors. Their size and cost make them ideally suited for portable and remote monitoring applications. Quantifying the sensor response, however, remains a significant challenge due to sensitivity to ambient temperature and humidity, and interference with non-target pollutant species. Temporal characteristics such as signal hysteresis and sensor drift over time also affect MOx sensor response.

We present a quantification model rooted in principles of semiconductor science and chemistry, yet informed by and simplified using empirical observations. This model predicts concentration from resistance while providing a correction for temperature effects, usually the most significant confounder in ambient air quality monitoring with MOx sensors, and drift due to change in the sensor heating element. The model parameter values are first determined using lab calibrations, then refined using a field collocation with reference instruments. The work thus provides both a quantification model and a means to effectively calibrate sensors for practical applications.

1. Introduction

The use of inexpensive sensor networks and embedded systems [1,2] are quickly emerging as a key player in the monitoring of local and regional air quality as lower cost monitoring equipment enables new spatial resolution of pollutants. Metal Oxide (MOx) type sensors [3,4] are one of several technologies being used in sensing gas phase pollutants. Many varieties of MOx sensors exist for the detection of different gas species. All types, however, function in a similar manner. An oxidation or reduction reaction occurs when species bind to the sensor surface resulting in the removal or injection of free electrical charge into the semiconductor material [5,6]. This process changes the sensor's electrical conductivity, which is measured by external instrumentation.

Unfortunately there are many challenges when trying to convert the sensor response to pollutant concentrations. All MOx sensors suffer from significant interference effects with temperature, humidity [7] and other gas species. Even when these parameters are controlled, the sensor conductivity is non-linear with respect to the gas species of interest. Most MOx sensors also exhibit 'out-of-the-box' variability from the manufacturing process. Finally, sensor signals will also drift over time from both poisoning (permanent bonding to the sensor surface) and changes in the sensor's heating element resistance caused by thermal stress.

Many approaches exist for the quantification of metal oxide gas sensor, yet most practical models are based entirely on experimentation and *a posteriori* knowledge of sensor behavior [8,9]. While these models provide acceptable results, they tend to be specific to sensor type and operating conditions. It would be advantageous to use a model derived entirely from the theory of chemistry and semiconductor physics, yet in practice this proves prohibitively complex. The approach presented here is rooted in the principles of semiconductor science, yet uses experimental observations to make informed assumptions and simplifications. Doing so retains some physical insight as to sensor behavior, yet allows the model to be tailored to sensor specific applications and proves to be effective in real-world implementation of ambient pollutant quantification.

The model derivation process consisted of lab experimentation and ambient collocation measurements. The theoretically derived model was first applied to experimental data, using the Sensortech (formerly e2v) MiCS-5525 as an example of a commercially available MOx type CO sensor. In practice, sensors are often employed in low pollutant concentration environments with significant environmental variability, hence the need to properly

* Corresponding author. Tel.: +1 5105062971.
E-mail addresses: nicholas.masson@colorado.edu (N. Masson), ricardo.piedrahita@colorado.edu (R. Piedrahita), hannigan@colorado.edu (M. Hannigan).

http://dx.doi.org/10.1016/j.snb.2014.11.032
0925-4005/

address temperature affects. Humidity effects were neglected as they are at least an order less significant than temperature effects, particularly for CO sensors [10].

MOx sensors are operated at elevated temperatures in order to facilitate the surface chemistry reactions of interest. Most commercially available MOx sensors have built in heating elements to keep the sensor surface in the vicinity of a target temperature. The resistance of the heating element and thus the heat output tend to change over time. This complicates the ambient temperature correction term as the relationship between surface temperature and ambient temperature is not constant when the heater output varies over time. To correct for this drift effect, the heater resistance was measured over several months and incorporated into the model as a temporally varying temperature correction term. This differs from other drift correction methods [11,12] as it is based directly on the observed changes in the sensor heater output. No drift due to poisoning was incorporated in the model, as drift of this type can only be accounted for by using periodic calibrations.

The sensors were then collocated with a reference carbon monoxide instrument in an urban environment. An optimization algorithm was used to dynamically fit the reference data to the theoretical model prediction, thus modifying the model parameters determined in lab experimentation.

2. Principles of MOx operation

Barsan and Weimar [13] present an in-depth discussion of the metal oxide semiconductor conduction model in which a sensor's conductivity is analytically attributed to changes in gas-phase species concentrations. Solving for the conductivity entirely from theory, however, requires extensive knowledge of the chemical kinetics and semiconductor electrical properties. Even if all parameters are known, the functional relationship between conductivity and ambient gas concentration requires numerically solving a complex system of several non-linear relations. Doing so is not practical in many applications; for our ambient application this approach is not feasible. It is thus necessary to incorporate simplifications and experimental data in the theoretical model derivation.

First consider the general principles driving MOx sensor operation. Fig. 1 is a simplistic representation of a MOx sensor element in an environment void of surface reactions. Pertinent attributes of the MOx element include the free charge density in the bulk material volume (charge that is free to conduct across the material), and the surface charge density (charge on the surface of the MOx sensor, which is free to react with reducing agents). The surface charge density will change with temperature.

Electrons are added or removed from the surface when the MOx sensor is exposed to reacting species. Chemical reaction theory governs these reactions. When charge is removed from the MOx surface, the bulk semiconductor responds by restoring some of the surface charge from the bulk charge 'reservoir'. This results in "band

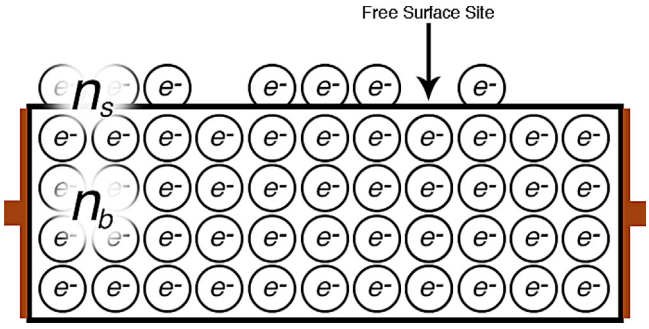

Fig. 1. MOx sensor without surface reaction.

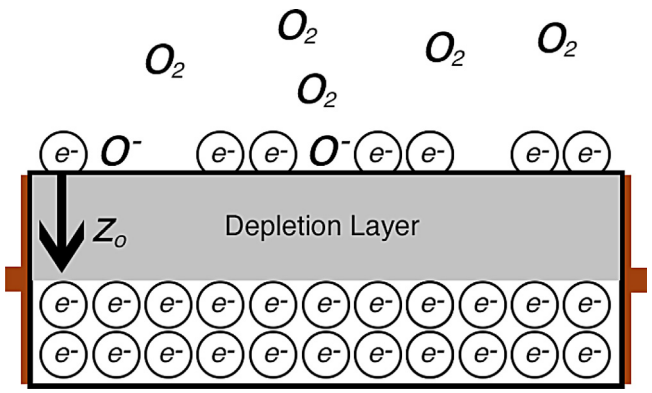

Fig. 2. MOx sensor with surface reaction.

bending" and depletion of some of the bulk charge within the semiconductor volume. As such, the surface charge provides the physical coupling between the semiconductor physics and the gas-phase surface chemistry. Fig. 2 is an example of a sensor element with a depletion layer due to atmospheric oxygen binding in its reduced form to the sensor surface.

Net conduction of electrons within the MOx element occur parallel to the sensor surface, whereas the depletion of charge occurs normal to the surface. It stands to reason then that the conductivity (or resistance) of the MOx sensor is a function of the depletion depth of charge within the bulk semiconductor.

Other important factors include the surface site concentration of chemisorbed species, the temperature dependence of chemical reactions and semiconductor band-bending, and the nature of intermediate and global reaction mechanisms. In this derivation, chemical reaction mechanisms are mostly neglected or generalized while temperature effects are more rigorously accounted for.

3. Model derivation

A usable model can be generated by applying practical simplifications to the theoretical derivation of a MOx sensor model. For our application, simplifications are motivated by a desire to have a closed-form, easily manipulated algebraic equation relating measurable quantities (resistance, ambient air temperature, etc.) with the concentration of target pollutants. The approximations used in this model are not necessarily the best or only approximations adequate for our application. A model derived from a different set of approximations may be equally valid. The model here represents one possible derivation, the quality of which is assessed in the final section. The focus here is on low detection limits where the sensor surface is far from being saturated with the target pollutant. The strong dependence of the sensor signal on sensor surface temperature (thus also ambient temperature) suggests the need for good fidelity between the final equation's temperature term and the governing equations driving the temperature affect.

To begin, it is assumed that the metal oxide semiconductor material is fabricated as a compact layer impermeable to gas-phase species. The metal-oxide crystals thus have tight grain boundaries with uniform imperfections over the volume of the sensing region. This supports the assertion that gas-phase reactions occur only with the exposed sensor surface and bulk charge transport (current in the sensor) traverses parallel to the sensor surface, whereas charge depletion due to surface reactions occurs normal to the semiconductor surface. This would not hold if the semiconductor were permeable to reactive gas species.

The conductivity of the semiconductor will depend on the depletion layer depth and the decrease in free charge density. Following Barsan and Weimar's derivation, the charge removed from the

depletion layer is taken to be equal to the charge captured by chemisorbed species at the semiconductors surface. This is known as the electroneutrality equation in the Shottky approximation and is given by Eq. (1) where ϕ is the species' ionization form, n_b is the bulk charge density in the semiconductor material and z_o is the depletion layer thickness normal to semiconductor surface. The bulk charge density n_b is assumed constant under steady operating conditions. Θ is the surface site coverage of chemisorbed species, which is defined as the sum of all occupied sites over the total surface site concentration, $[S_t]$ for which gas-phase species compete.

$$\phi \cdot \Theta \cdot [S_t] = n_b \cdot z_0 \tag{1}$$

If, as the electroneutrality equation suggests, the depletion layer is void of all free charge carriers, then only the bulk charge n_b in the non-depleted layer contributes to the semiconductor conductivity. Here the conductance, G_s is taken to be proportional to the non-depleted region and scaled by a characteristic length, L. The characteristic length describes the transverse direction across which conduction occurs, and is sensor specific. This in part explains inter-sensor variability as a product of inconsistencies in sensor manufacturing.

$$G_s = \gamma \cdot \quad n_b \cdot L \cdot (h - z_o) \tag{2}$$

Here h is the semiconductor thickness and γ is an unknown constant of proportionality.

Calculating the surface site coverage Θ in Eq. (1) requires extensive knowledge of the reaction mechanisms and chemical properties governing surface and gas phase reactions. A simplified form assumes atmospheric gas phase reactants to bind directly with free surface electrons on the sensor surface:

$$S + \alpha \cdot e^- + C_{(g)} \rightleftharpoons C_{(s)}^{-\alpha} \tag{3}$$

where S is the number of unoccupied sites, e^- are free surface electrons whose concentration is herein after denoted $[n_s]$ and $[C_{(g)}]$, $[C_{(s)}]$ are gas phase and chemisorbed reactants, respectively. If the surface sites are predominantly occupied by one gas phase reactant (typically oxygen), and it is assumed that $\Theta \ll 1$, then Eq. (3) gives:

$$\Theta = \frac{k_f}{k_r} \cdot [C_{(g)}] \cdot [n_s] \tag{4}$$

where k_f and k_r are the forward and reverse rate constants, respectively, and it is further assumed that the reaction is of first order in its reactants. The forward and reverse rate constants are given by the Arrhenius rate equation:

$$k = A \cdot \exp\left(-\frac{E_a}{k_B T}\right) \tag{5}$$

where E_a is the reaction activation energy, k_B is the Boltzmann constant, and T is the semiconductor temperature.

Combining Eq. (1) with Eq. (4) and assuming that the reactants are singly ionized, gives:

$$z_o = \frac{[S_t]}{n_b} \cdot \frac{k_f}{k_r} \cdot [C_{(g)}] \cdot [n_s] \tag{6}$$

The surface charge density n_s is related to the semiconductor band bending qVs and, similar to the Arrhenius equation, is given by:

$$n_s = n_b \cdot \exp\left(-\frac{qV_s}{k_B T}\right) \tag{7}$$

The surface band bending can be calculated as per Barsan and Weimar [13] by solving the Poisson equation, giving:

$$qV_s = \frac{q^2 \cdot n_b}{2 \cdot \epsilon \cdot \epsilon_0} \cdot z_0^2 \tag{8}$$

Eq. (8) can be simplified by assuming that in most ambient environments concentrations are low enough that band bending varies linearly rather than quadratically with z_o. This allows qVs to be expressed as:

$$qV_s = -\xi \cdot z_o \tag{9}$$

where ξ is a proportionality constant.

Combining Eq. (6) with Eqs. (7) and (9) allow z_o to be expressed as:

$$z_o = [S_t] \cdot \frac{k_f}{k_r} \cdot [C_{(g)}] \cdot \exp\left(\frac{\xi z_o}{k_B T}\right) \tag{10}$$

A closed form solution using the Lambert W function gives z_o as:

$$z_o = -\frac{k_B T}{\xi} \cdot W\left([S_t] \cdot \frac{k_f}{k_r} \cdot [C_{(g)}] \cdot \frac{\xi}{k_B T}\right) \tag{11}$$

Unfortunately the Lambert W function is ill-suited for algebraic manipulation and general model implementation. In practice, the unknown coefficients are determined experimentally, so one need only be concerned with preserving model form and modes of non-linearity. It was found that an exponential function would suffice in lieu of the Lambert W function. That is, there exists coefficients $\{a, b\}$ such that $a\exp(bx)$ adequately captures the non-linearity in $W(cx)$ over some range of interest $\{x_1, x_2\}$. The physical meaning in the constant coefficient values is lost when $c \rightarrow \{a, b\}$. Combining the above approximation with Eqs. (11), (2), (5), allows for the conductance to be written as a function of temperature and atmospheric reactant concentration as:

$$G_s/L = a_1 - a_2 \cdot T \cdot \exp\left(\frac{a_3 \cdot [C_{(g)}]}{T^2}\right) \tag{12}$$

For a carbon monoxide (CO) sensor, CO acts as a reducing agent, binding to oxygen groups already chemisorbed to the surface. The result is to return free charges to the semiconductor previously removed by the oxygen bonds. Barsan and Weimar [13] present a rigorously derived closed form solution for conductivity as a function of ambient CO partial pressure. Here, however, we will make use of the simplified conductivity equation Eq. (12) and allow $[C_{(g)}] \rightarrow a_4 + a_5 \cdot [CO]$. In this case, a_4 is a proxy for chemisorbed oxygen and a_5 describes a linear propensity for CO to remove the chemisorbed oxygen. The surface sites occupied by oxygen are assumed to be constant, any change due to atmospheric variability being negligible relative to the CO effect.

The final model gives free parameters to all unknown constants. The values of the constants are determined experimentally, and can generally characterize the behavior of all sensors of a given type after accounting for inter-sensor variability. The validity of the above assumptions are investigated in experimental observation.

4. Experimental setup

An array of three Sensortech (formerly e2v) MiCS-5525 carbon monoxide sensors were placed in an aluminum enclosure and attached to an inlet mixing manifold. Three mass flow controllers (MFCs), controlled by a custom LabView VI, fed dry air, humid air and a 1018 ppm carbon monoxide (CO) gas standard into the mixing manifold to achieve six levels of CO concentration between zero and 2.8 ppm. The air used was zero grade, provided by Airgas, while the CO standard was supplied by Air Liquide. A heat lamp was duty cycled by the LabView VI to control ambient gas temperature within the enclosure. A given sample run lasted approximately three hours and consisted of holding the inlet CO concentration and absolute humidity constant while cycling through different temperature levels. The temperature was held at five set points between 298 and 315 K. There were six sample runs in total each with a different

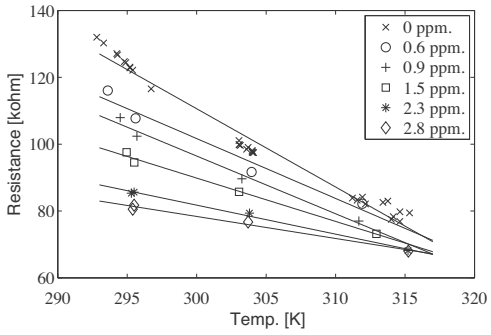

Fig. 3. MiCS-5525 response to temperature at various CO concentrations.

carbon monoxide level at concentrations of {0, 0.6, 0.9, 1.5, 2.3, 2.8} ppm. The three sensor signals were collected at a 1 Hz frequency using a LabJack 10 bit analog-to-digital converter, and the temperature and relative humidity was recorded using a Sensirion SHT-11 relative humidity and temperature sensor.

5. Experimental results and parameter estimation

Sensor resistances were extracted from the LabView log file data for each sensor at various temperature levels for the six runs. The sensor response was assumed to be at steady state with respect to CO for any given run. Absolute humidity was held at 0.015 [mol/mol] (equiv. 40%Rh at 25 °C) for all runs.

The response of the MiCS-5525 sensor, as shown in Fig. 3, was close to linear in temperature over all concentration levels.

It is common practice to normalize the signal resistance by a sensor-specific constant value. Doing so helps to account for inter-sensor variability as shown in Fig. 4, the physical basis of which is previously discussed in the derivation of Eq. (2). Inter-sensor variability is considered to be the variability in signal output for identical sensors in an identical environment. Fig. 4 shows the difference in sensor response from three MiCS-5525 sensors when exposed to an identical zero air environment.

Each sensor was given a resistance values, R_o, defined as the resistance of the sensor at 298 K in zero air. These values were taken from the linear regression of resistance versus temperature at zero concentration for each of the three sensors. A normalization procedure by which each sensors' resistance is divided by its R_o value gives good inter-sensor agreement as seen in Fig. 5.

The adjusted R^2 for the least-squares linear fits to the normalized sensor data ranges from 0.9724 to 0.9879 (each a mean value for the three sensors), increasing monotonically with concentration. This improvement of fit with concentration coincides with the observation that the response data becomes more linear with temperature as concentration is increased. The p-values for all fits were below 0.05. The measured resistance is related to the derived

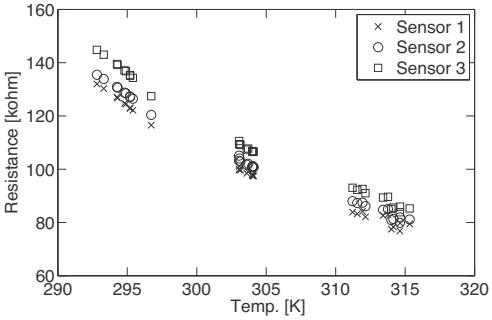

Fig. 4. MiCS-5525 inter-sensor variability for three sensors at zero concentration.

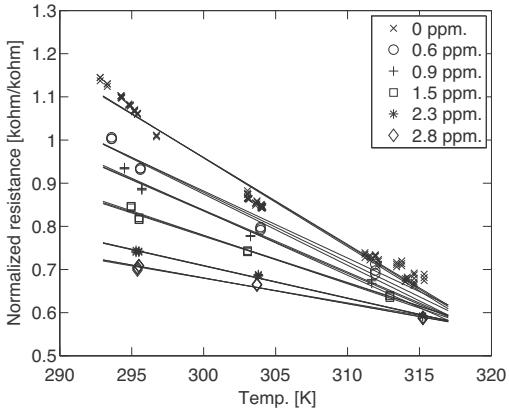

Fig. 5. Normalized resistance of three MiCS-5525 sensors.

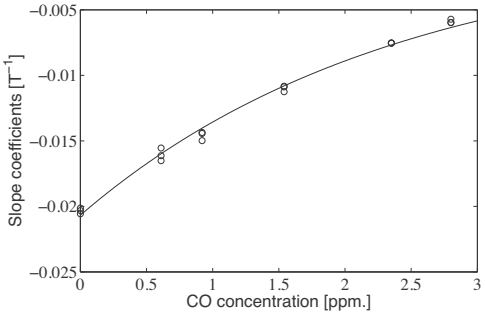

Fig. 6. MiCS-5525 temperature slope coefficients.

conductivity model Eq. (12) by the reciprocal relationship $\sigma = \rho^{-1}$ between conductivity and resistivity. It was found that neglecting the reciprocal term and taking conductivity to decrease proportionally to resistivity provided sufficient results. Then linearizing Eq. (12) with respect to temperature at 298 K based on observations in Fig. 3 gives the model form used for the MiCS-5525 sensor:

$$R_s = (p_1 + p_2 \cdot [\mathrm{CO}]) \cdot \exp(p_3 \cdot [\mathrm{CO}]) \cdot (T - 298) + p_4 \cdot \exp(p_5 \cdot [\mathrm{CO}]) + p_6 \quad (13)$$

Using Eq. (13), the pseudo-intercepts (defined as the normalized resistance at 298 K) were determined from each sensors' linear regression at each concentration level. The slope term, $(p_1 + p_2 \cdot [\mathrm{CO}]) \cdot \exp(p_3 \cdot [\mathrm{CO}])$, and the pseudo-intercept term, $p_4 \cdot \exp(p_5 \cdot [\mathrm{CO}]) + p_6$, were then fit to the experimental data using a least-squares approach as shown in Figs. 6 and 7. The adjusted R^2 for the slope coefficient and pseudo-intercept coefficient fits are

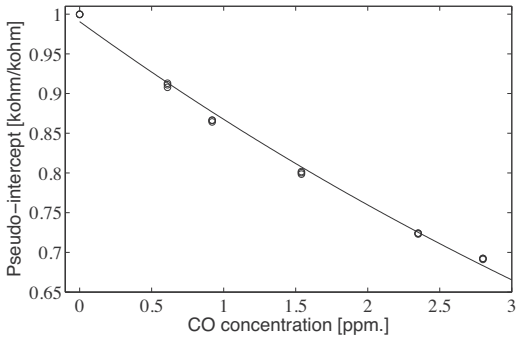

Fig. 7. MiCS-5525 temperature pseudo-intercept coefficients.

1.000 and 0.965, respectively, with p-values below 0.05. It should be noted that these fit statistics pertain to two independent elements of the model, thus do not represent the quality of the whole model fit, as discussed in the final section.

The parameters generated in the lab experiment predict CO concentration well under lab conditions, yet still present difficulties when implemented in real-world applications.

6. Sensor heater drift

Temperature plays a significant role in the sensor output and must be compensated for in any MOx quantification model where temperature is not constant. For example, it is well known that the sensor temperature may be actively modulated to alter a sensor's gas sensing characteristics [14,15]. In this application, the sensors have a constant excitation voltage applied as per the spec sheet. As a result, the MOx sensors exhibit heater drift in which the resistance of the heating element in the sensor will drift over time. This is a common problem with MOx sensors in systems where the heater is not actively controlled. When the heater resistance changes so too does the heater power output and thus the sensor surface temperature.

The ambient air temperature is directly related to the sensor surface temperature by the convective heat transfer equation:

$$Q(t) = h_t \cdot (T_s - T_a) \tag{14}$$

where T_s is the sensor surface temperature, T_a is the ambient temperature, $Q(t)$ is the time varying sensor heater output and h_t is the convective heat transfer coefficient. When $Q(t)$ and h_t do not change, the ambient temperature scales directly with the surface temperature. It is assumed that h_t is constant under steady ambient air flow (e.g. a constant flow of air over the sensor from an inlet fan).

The power output from the heater resistor is a function of the heater resistance, $R_h(t)$, and the voltage drop across the resistor, $V_h(t)$, given by:

$$Q(t) = \frac{V_h^2(t)}{R_h(t)} \tag{15}$$

The voltage drop across the resistor depends on the excitation voltage, V, and the voltage divider resistor value, R_{hd}, given by:

$$V_h(t) = V \cdot \frac{R_h(t)}{R_h(t) + R_{hd}(t)} \tag{16}$$

The changes in heater resistance for four MiCS-5525 sensors were measured over a 250+ days period. The resistance was consistent across the four sensors, the difference in heater resistance being within the measurement error. The drift in heater resistance over time for one sensor is shown in Fig. 8. Note that the discrete steps in resistance are due to the sampling resolution, and intermediate data points being due to the daily averaging process. It is also assumed that the drift in heater element resistance is due to heater degradation and not the dependence of the heater element resistance on temperature. The heater drift experiment was conducted indoors where ambient temperature and humidity are stabile, and no significant covariance was observed between ambient temperature and the heater element drift.

A second order polynomial of the form:

$$R_h(t) = a_1 + a_2 \cdot t + a_3 \cdot t^2 \tag{17}$$

was fit to the heater resistance data using a least-squares method. The polynomial was fit piecewise to the first 30 days in which the greatest change in heater resistance was observed, and then again to the period of 30+ days. Doing so for the four sensors gives mean adjusted R^2 values ranging from 0.91 to 0.98 for the 0–30 days period and 0.990–0.992 for the 30+ days period. All p-values were below 0.05.

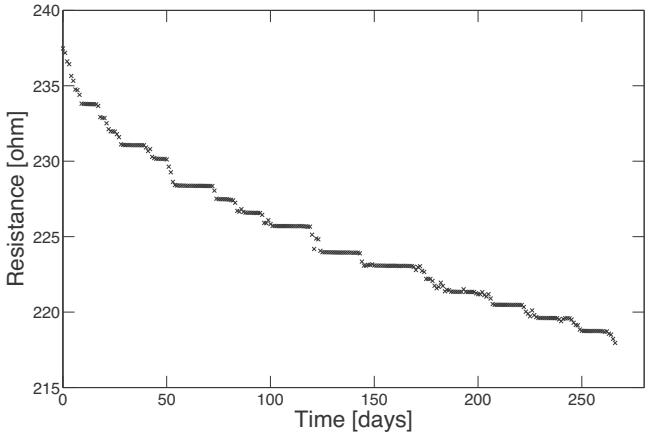

Fig. 8. MiCS-5525 heater resistance drift over time.

$Q(t)$ is then given by Eqs. (15)–(17).

Eq. (14) can be rewritten:

$$Q_o = h_t \cdot (T_s - T_a + \Delta Q_h / h_t) \tag{18}$$

allowing the change in heater output ΔQ_h, where $\Delta Q_h = Q_h(t) - Q_h(0)$, to manifest itself as a correction to the ambient temperature measurement:

$$T_a^* = T_a - \frac{\Delta Q_h}{h_t} \tag{19}$$

Equation Eq. (19) gives a modified temperature term when $T \rightarrow T_a^*$ in the sensor resistance model Eq. (13). Note that the convective heat transfer coefficient is unknown and must be determined experimentally.

7. Collocation setup

Two U-Pod embedded systems were each outfitted with 4 MiCS-5525 CO sensors and collocated with a Thermo Scientific Model 48 reference instruments at the CDPHE CAMP site for 19 days during April 2013. The monitoring station is located at a busy intersection in downtown Denver at 2105 Broadway St. The monitoring station is adjacent to a busy motorway resulting in moderately high pollutant concentrations during rush hour periods. The reference instrument provided a dynamic concentration reading for the examination of discrepancies between sensor operation in the lab and in the field. The U-Pods were placed near the reference instrument inlet on the roof of the monitoring station. The U-Pods were powered continuously, and had small fans installed to provide air flow through the enclosures. The temperature and humidity was also measured in the U-Pod system enclosure. The sensor resistances, relative humidity and temperature were sampled at 0.3 Hz and averaged over one minute periods.

8. Collocation results and parameter optimization

During the collocation, the temperature within the U-Pod enclosure over this period varied from 0 to 35 °C with an average temperature of 14 °C. The absolute humidity mol fraction in the enclosure varied from 0.003 to 0.011 mol/mol with an average of 0.007 mol/mol.

A predicted resistance was calculated using Eq. (13) with the collocation reference concentration and the lab generated parameters. Fig. 9 shows the predicted versus measured resistance for one MiCS-5525 sensor. Each data point corresponds to a one minute

Table 1
Optimized parameter values and prediction of error.

Sensor #	R_o	p_1	p_3	p_4	p_5	p_6	h_t	RMS [kohm]
Lab	N/A	−02.07e−02	−4.21e−01	9.90e−01	−1.33e−01	9.00e−04	N/A	N/A
1	101.96	−1.09e−02	−5.26e−01	5.47e−01	−3.01e−01	4.81e−01	9.46e−06	2.98
2	96.02	−1.13e−02	−4.91e−01	4.93e−01	−3.03e−01	5.31e−01	1.13e−05	2.73
3	120.54	−1.39e−02	−6.76e−01	4.88e−01	−4.08e−01	5.46e−01	1.01e−05	3.40
4	121.99	−1.28e−02	−6.51e−01	4.51e−01	−4.26e−01	5.81e−01	9.78e−06	3.37
6	114.44	−1.04e−02	−5.73e−01	6.20e−01	−3.21e−01	4.12e−01	8.18e−06	3.47
7	108.08	−1.02e−02	−5.74e−01	6.13e−01	−3.00e−01	4.15e−01	8.92e−06	3.10
8	117.70	−9.97e−03	−5.75e−01	6.33e−01	−3.16e−01	4.00e−01	7.52e−06	3.36

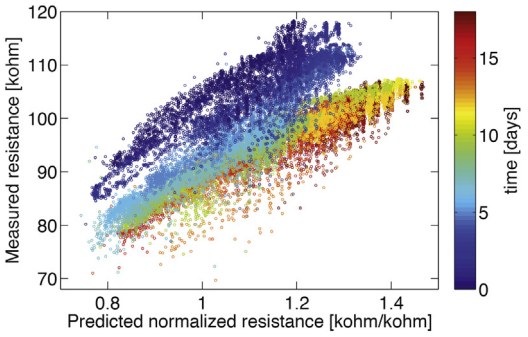

Fig. 9. MiCS-5525 measured vs. predicted resistance with lab parameters.

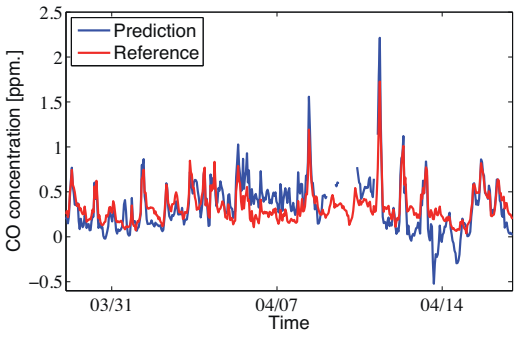

Fig. 11. Comparison of predicted and actual concentration.

average over the 19 days period. No R_o normalization factor or sensor heater drift compensation was used in the initial prediction.

The lab parameters do well in linearizing the relationship between the predicted and measured resistance, yet it can be seen that significant temporal drift exists when there is no compensation for the change in heater resistance.

Optimal parameters were generated using the NonLinearModel fitting algorithm in Matlab and minimizing the residual between observed and predicted sensor resistance. The model form Eq. (13) was again used to predict sensor resistances, except the constant coefficients $p_1, \ldots, p_6$ and the heat transfer coefficient h_t were set as free parameters in a least-squares fit of the predicted resistance to the measured resistance. The heater drift correction was also applied to the temperature term as per Eq. (19). Doing so gave very good agreement between the measured and the predicted resistance as shown in Fig. 10, with an adjusted R^2 of 0.88 and p-value for all parameters below 0.05. The variable space for this model fit is comprehensive enough in span (temperature, concentration, etc.), that the free parameters are assumed to be statistically significant for any realistic variable space to which the model is fit. Similarly, it is possible that a less generalized model with a subset of parameters would suffice for a more constrained variable space, such as when used in a climate controlled building.

Table 1 gives the model parameters from the initial lab experiment and those from the optimization scheme applied to the collocated sensors. Note that p_2 was omitted from the model after initial investigation proved it be sufficiently small as to not contribute to fit quality, and only seven sensor results are presented as one of the collocated sensors broke while in the field.

The value of R_o presented in the table was generated by evaluating the model at 298 K with a concentration of zero. Using a numerical solver to compute the concentration over the 19 days period gives an RMS error in ppm carbon monoxide ranging from 0.22 to 0.48. It should also be noted that high frequency spikes of carbon monoxide appear in the reference data due to intermittent point sources in the vicinity of the reference station (e.g. passing cars). Differences between the reference instrument and U-Pod in air exchange rate, flow transit time and response time mean that high frequency spikes in pollutants do not always line up temporally, which sometimes contributes to more significant error when fitting to reference data. This issue is of less concern when dealing with pollutants and sensors in a less dynamic environment (e.g. diurnal cycles in ozone).

Fig. 11 shows the predicted versus reference concentration for one sensor over the 18 days collocation period. Note that most of the sensor data was lost on April 4th. This period of time in early spring is particularly dynamic as temperatures vary significantly from night to day, as shown in Fig. 12. It can be seen that the agreement between the sensor and the reference instrument is

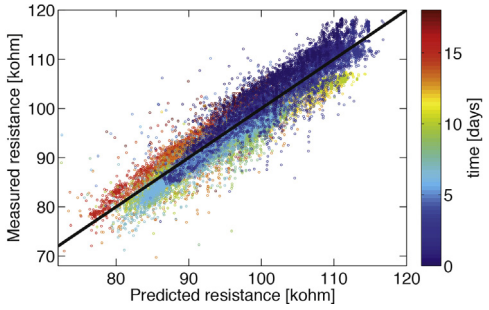

Fig. 10. MiCS-5525 measured vs. predicted resistance with optimized parameter.

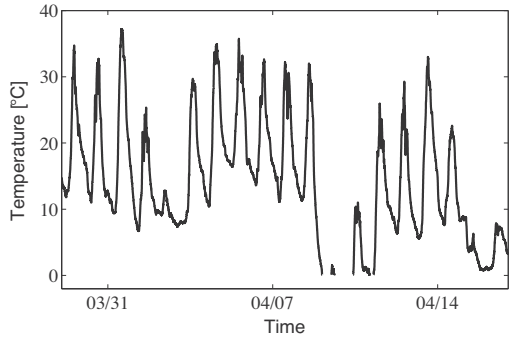

Fig. 12. Temperature during collocation period.

particularly poor on April 6th. This is likely due to a large storm event and intermittent precipitation. The slight humidity effect is also apparent in the baseline shift as the 6 days mean absolute humidity mol ratio slowly shifted from 0.072 to 0.064 back to 0.072 over the 18 days period.

9. Conclusions

The model form derived in this work does well to predict the sensor response to ambient pollutants while compensating for temperature affects and sensor drift due to changes in the sensor heating element. All sensors of a given type work well with the same model form, yet significant inter-sensor variability requires each sensor to have a unique set of parameter values. Parameter values determined in a lab setting perform poorly when the sensors are deployed in the field. Collocation calibrations are superior in generating optimal model parameter values. The drift of the heating element output must be known in order to compensate for heater drift. This can be achieved by incorporating heater drift in the quantification model, or measuring and adapting the heater output *in situ*.

Future models should build upon the foundation presented here, incorporating further corrections for humidity, pressure, and interference species. Promising approaches include the use of redundant sensors and arrays of sensors with different interference cross-sensitivities.

References

[1] J. Li, B. Faltings, O. Saukh, D. Hasenfratz, J. Beutel, Sensing the air we breathe – the OpenSense Zurich dataset, in: Proceedings of the 26th AAAI on Artificial Intelligence, 2012, pp. 2–4.
[2] V. Jelicic, S. Member, M. Magno, D. Brunelli, G. Paci, L. Benini, Context-adaptive multimodal wireless sensor network for energy-efficient gas monitoring, IEEE Sens. J. 13 (1) (2013) 328–338.
[3] X. Liu, S. Cheng, H. Liu, S. Hu, D. Zhang, H. Ning, A survey on gas sensing technology, Sensors (2012) 9635–9665.
[4] Y. Sun, S. Liu, F. Meng, J. Liu, Z. Jin, Metal oxide nanostructures and their gas sensing properties: a review, Sensors (2012) 2610–2631.
[5] M. Gardon, J.M. Guilemany, A review on fabrication, sensing mechanisms and performance of metal oxide gas sensors, J. Mater. Sci. Mater. Electron. 24 (2013) 1410–1421.
[6] G.F. Fine, L.M. Cavanagh, A. Afonja, R. Binions, Metal oxide semi-conductor gas sensors in environmental monitoring, Sensors (2010) 5469–5502.
[7] N. Barsan, U. Weimar, Understanding the fundamental principles of metal oxide based gas sensors; the example of CO sensing with SnO_2 sensors in the presence of humidity, J. Phys.: Condens. Matter 15 (2003) R813.
[8] H. Baha, Z. Dibi, A novel neural network-based technique for smart gas sensors operating in a dynamic environment, Sensors (2009) 8944–8960.
[9] M. Kamionka, P. Breuil, C. Pijolat, Calibration of a multivariate gas sensing device for atmospheric pollution measurement, Sens. Actuators B 118 (1–2) (2006) 323–327.
[10] R. Ionescu, A. Vancu, A. Tomescu, Time-dependent humidity calibration for drift corrections in electronic noses equipped with SnO_2 gas sensors, Sens. Actuators B (2000) 283–286.
[11] J.-e. Haugen, O. Tomic, K. Kvaal, A calibration method for handling the temporal drift of solid state gas-sensors, Anal. Chim. Acta 407 (2000) 23–39.
[12] A. Vergara, S. Vembu, T. Ayhan, M.a. Ryan, M.L. Homer, R. Huerta, Chemical gas sensor drift compensation using classifier ensembles, Sens. Actuators B 166–167 (2012) 320–329.
[13] N. Barsan, U. Weimar, Conduction model of metal oxide gas sensors, J. Electroceram. (2001) 143–167.
[14] R. Gosangi, R. Gutierrez-osuna, Active temperature modulation of metal-oxide sensors for quantitative analysis of gas mixtures, Sens. Actuators B 185 (2013) 201–210.
[15] J. Fonollosa, L. Fernández, R. Huerta, A. Gutiérrez-gálvez, S. Marco, Temperature optimization of metal oxide sensor arrays using mutual information, Sens. Actuators B 187 (2013) 331–339.

Biographies

Nick Masson is a professional research assistant at the University of Colorado at Boulder. His work focuses predominantly on the implementation of remote sensing technology, including the experimental design and modeling for a multivariate response of environmental sensors to both target pollutants and interference factors. He received his MS in Mechanical Engineering from the University of Colorado at Boulder. His Master's thesis involved modeling methods for low cost sensors and computational modeling of combustion processes in biomass cookstoves. Recent projects include the development of affordable air quality monitors designed for remote data acquisition, with applications in global and domestic studies.

Ricardo Piedrahita is a PhD student in Mechanical Engineering at the University of Colorado Boulder. His research focus is on low-cost air quality monitoring. Ongoing research includes a project in Northern Ghana performing personal, microenvironmental, and regional air quality measurements as part of a cookstove intervention study. In addition to cookstove research, he is interested in quantification and uncertainty estimation for low cost air quality sensors, as well as engineering solutions for widespread adoption of such technologies. Before starting his PhD work, he received a BS in Mechanical Engineering at the University of California San Diego, and later a MS in Mechanical Engineering at the University of Colorado Boulder. His Master's thesis covered source apportionment of fine particulate matter in Denver Colorado, and non-parametric regression of coarse particulate matter for trend and source identification in urban and rural locations in Colorado.

Michael Hannigan is an Associate Professor of Mechanical Engineering at the University of Colorado. His research activities are focused on air quality characterization leading to improving human and ecosystem health. He has 25 years of experience at collection, characterization, and source attribution of airborne particulate matter. In the past five years, his group has moved into development of low-cost monitoring tools which are now being applied to technology assessment in the developing world as well as energy development and use in the Rocky Mountain region of the US.